# High-Mass Matrix-Assisted Laser Desorption/Ionization Mass Spectrometry for Absolute Quantitation of Noncovalent Protein–Protein Binding Interactions

**Author(s):**
Wu, Na ⬤; Jiao, Lingyi; Bütikofer, Matthias; Zeng, Zhihui; Zenobi, Renato ⬤

# Supporting information

**High-mass MALDI mass spectrometry for absolute quantitation**

**of noncovalent protein-protein binding interactions**

*Na Wu,[†] Lingyi Jiao,[†] Matthias Bütikofer,[†] Zhihui Zeng,[‡ §] Renato Zenobi[*, †]*

[†]Department of Chemistry and Applied Biosciences, ETH Zurich, CH-8093 Zurich, Switzerland.
‡ School of Materials Science and Engineering, Shandong University, Jinan 250061, PR China.
§ Empa, Swiss Federal Laboratories for Materials Science and Technology, Überlandstrasse 129, Dübendorf, 8600 Switzerland.
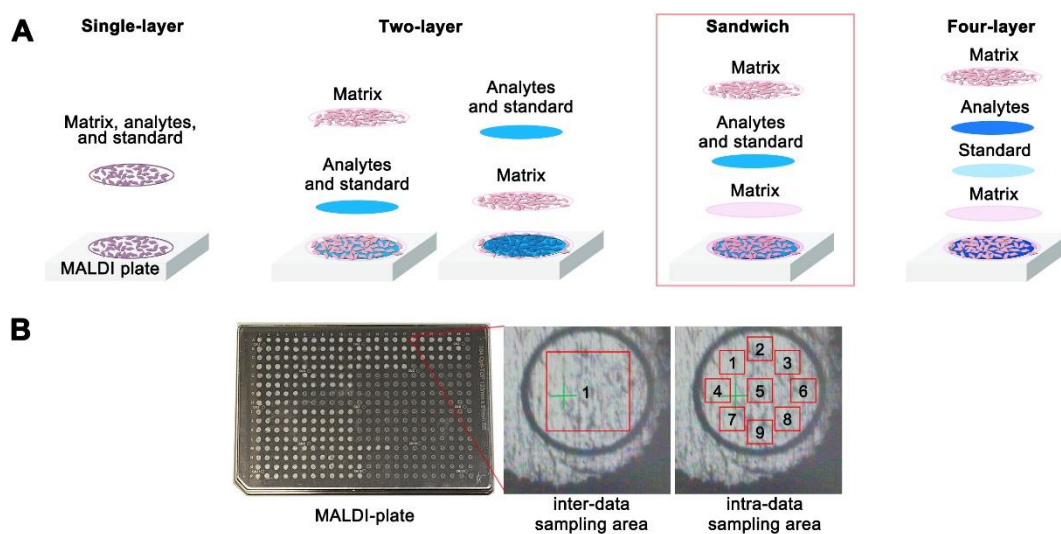
**Figure S1.** (**A**) Illustration of the four methods of applying standards that were tested for quantitative high-mass MALDI-MS. The one-layer method requires the premixing of matrix and analyte-standard mixture. In the two-layer method the matrix and analyte-standard mixture are deposited on the spot separately. In the three-layer method the analyte-standard mixture is sandwiched between two layers of matrix. The four-layer requires one to deposit the matrix, standard, analytes, and matrix, in order from bottom to top. (**B**) Different sampling areas for the acquisition of inter-data (a square scan area in one spot, scan once for one spot, and totally scan 8 spots for one sample) and intra-data (nine different square scan areas in one spot, totally scan nine times for one spot) using MALDI-MS.
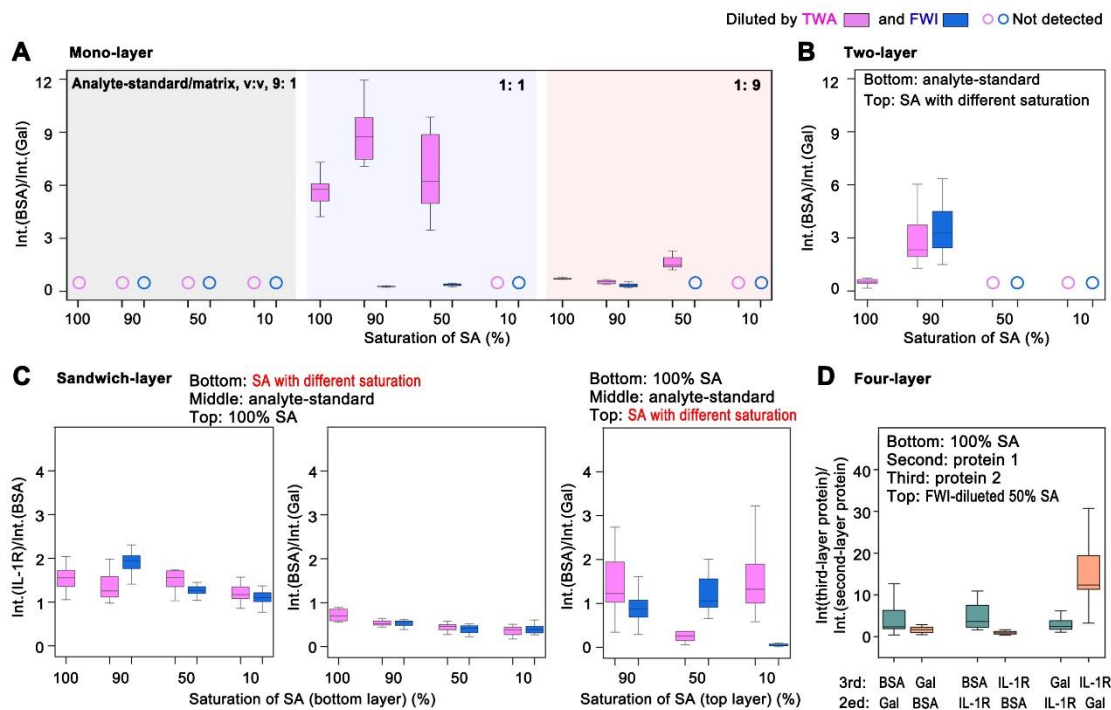
**Figure S2.** Boxplots showing peak intensities (25th-75th percentile with the median) ratios of analyte to internal standard protein measured by the mono-layer (**A**), two-layer (**B**), sandwich (**C**), and four-layer (**D**) deposition methods, respectively. The error bar corresponds to $1.5 \times$ IQR. n=8 (data was collected from 8 sample spots).

## Evaluation of deposition methods and factors affecting signal stability.

As shown in Figure 2A and S2, for the mono-layer deposition method (Figure S1), CV values calculated from inter- and intra-spot data are comparable. When using a volume ratio of analyte-standard/SA, 9:1, no signal was detected (Figure 2A). This can be attributed to that the quantity of matrix being too low, such that the matrix could not co-crystalize with the proteins. For a volume ratio of analyte-standard/SA, 1:1, the CV values of FWI-diluted 90% and 50% SA samples were significantly lower than those of 100%, TWA-diluted 90%, and TWA-diluted 50% SA samples (Figure 2A). As illustrated in the SEM images (Figure 2B and Figure S3A), seed-like, homogenous and ordered microscale crystals were formed with the addition of a more volatile solution of FWI. Without FWI, we did not observe clear crystals for 100% SA samples, and local agglomerations were formed for 90% and 50% SA samples. For the volume ratio of analyte-standard/SA, 1:9, the CV values of 100%, TWA-diluted 90%, and TWA-diluted 50% SA samples were much lower than those of the FWI-diluted 90% and 50% SA samples. The SEM images (Figure S3) showed that the 100%, TWA-diluted 90%, and TWA-diluted 50% SA samples had ordered and dense leaf-like crystals. However, the FWI-diluted 90% SA samples only had a few scattered crystals, and there

40  was almost no crystal formation in the FWI-diluted 50% SA samples. To be concise, for mono-

41  layer deposition method, the peak integral ratio of the analytes to standard (Figure S2) and the

42  stability of the peak integral ratio of analyte to standard (Figure 3A) were influenced by the volume

43  ratio of protein solutions to SA solutions and the saturation of SA. Moreover, samples with a leaf-

44  like crystal morphology showed more stable signals than those with a seed-like crystal morphology

45  (Figure 2A and S3).

46  Compared to the one-layer deposition method, loading the matrix and analytes separately is more

47  suitable for high-throughput detection. In this way, we do not need to premix the matrix with the

48  analytes and the dilution of the analytes is avoided. A saturated bottom layer of SA formed dense

49  and well-ordered leaf-like crystals. With the dilution of TWA solution, sparse needle-like crystals

50  were formed, while with the addition of the same amount of FWI solution, amorphous film was

51  formed. (Figure S4A). The deposition of the protein solutions (BSA-Gal mixture) did not induce

52  any morphological changes of the bottom-layer (Figure 2E). However, no signal was detected in

53  this two-layer deposition way (bottom layer: SA, top layer: analyte-standard). We believe that this

54  can be attributed to a shielding effect of the matrix on the bottom by the proteins on top, which

55  probably obstructs the energy transfer from the laser to the SA crystals. After reversing the

56  deposition order of protein and matrix, signals were detected when the saturation of SA was 100%

57  or 90% (diluted by TWA and FWI), but they were not stable (CV> 20%) (Figure 2B and 2F).
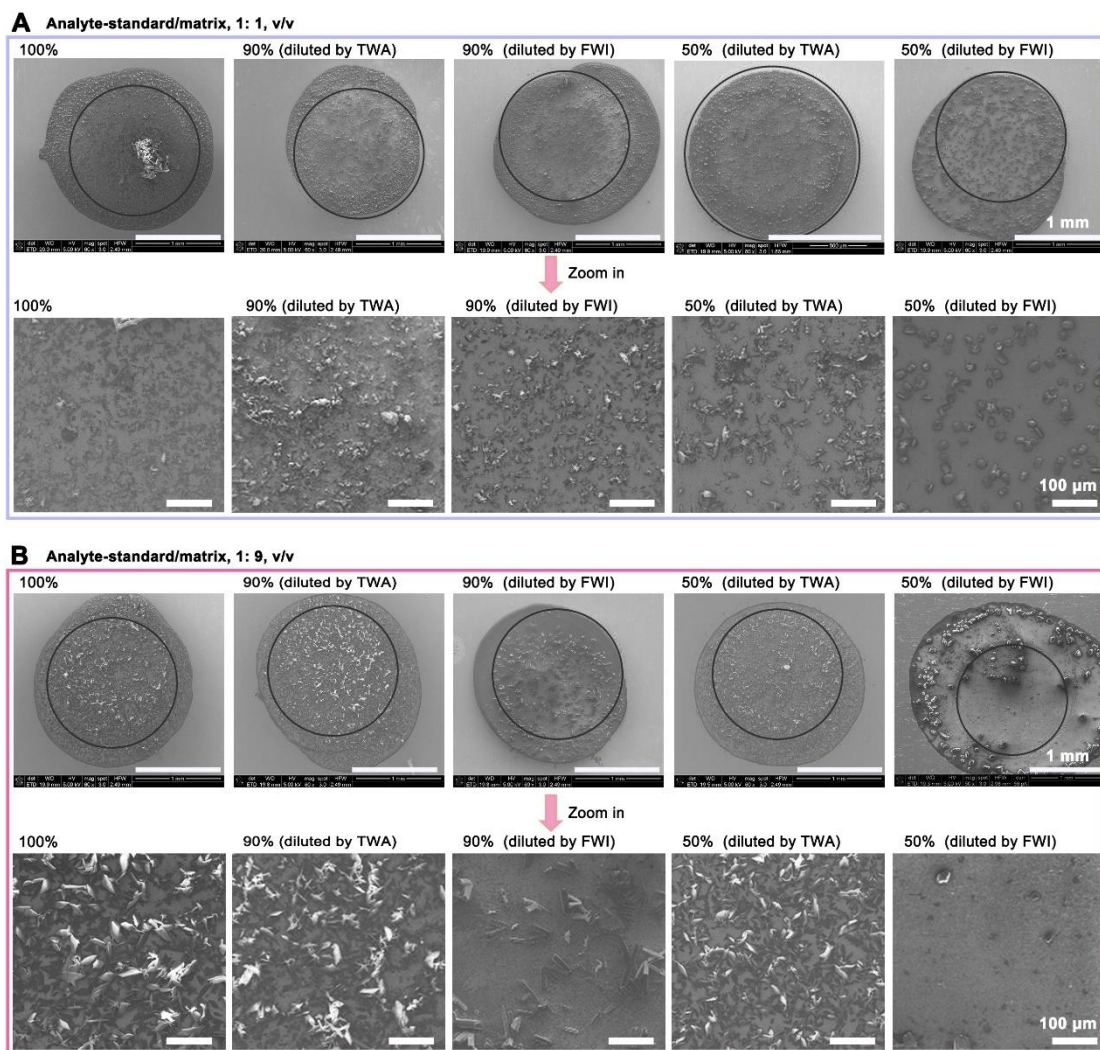
**Figure S3.** SEM images of the samples on the MALDI spot using one-layer deposition method with different matrix saturations and different analyte/matrix volume ratios. The volume ratio of analyte and standard mixture to the SA solution was 1: 1(**A**) and 1:9 (**B**). From left to right, the saturation of the SA was 100% (dissolve in 1:500:500 v/v/v TFA/water/acetonitrile solution (TWA)), 90% (diluted by TWA and 2:1:3 v/v/v formic acid/water/isopropanol solution (FWI) separately), and 50% (diluted by TWA and FWI separately).Scale bar: 1mm (zoom out) and 100 μm (zoom in).
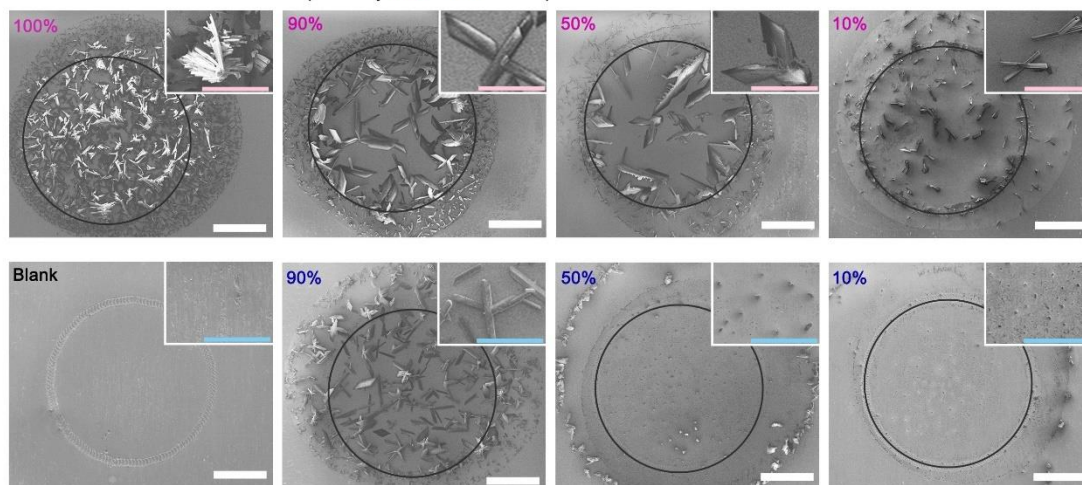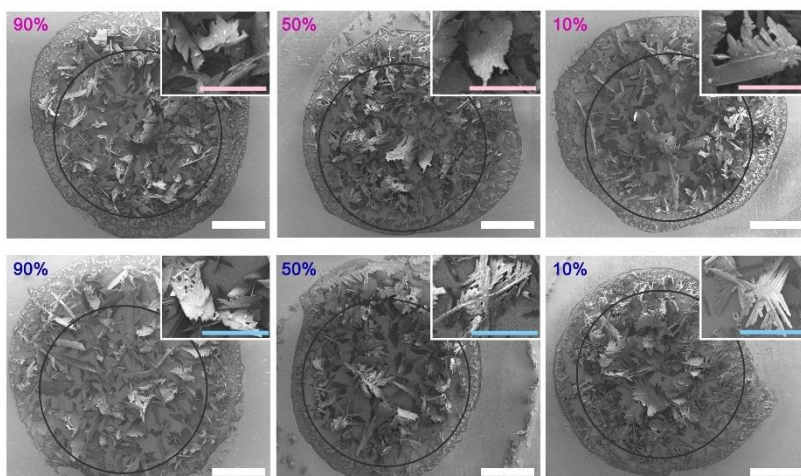
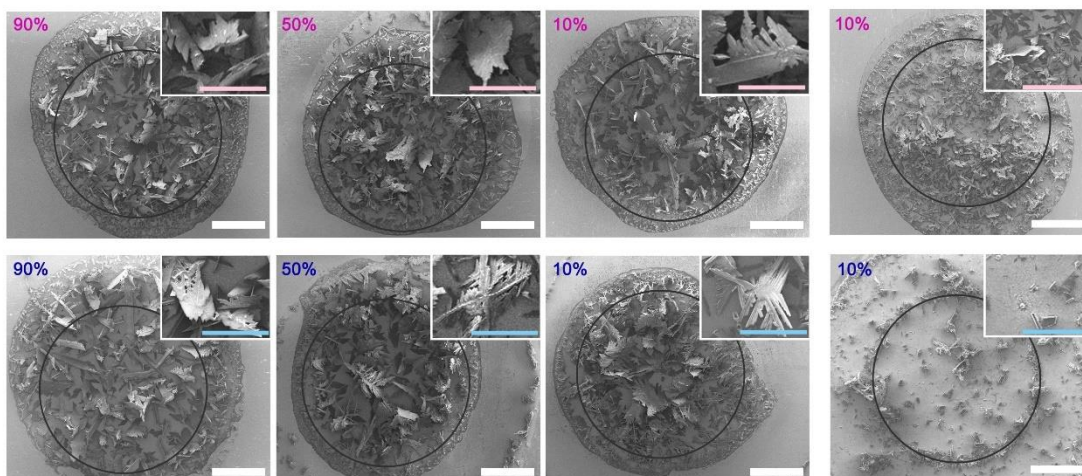**Figure S4.** SEM images of the samples on MALDI spot after using different deposition methods. (**A**) One layer of SA on the MALDI spot. The saturation of SA from left to right was 100%, 90%, 50%, 10%, diluted by TWA (top row) and FWI (bottom row), respectively. Blank spot was a control. The inserted image was an enlarged view of the SA crystal in each spot. A saturated bottom layer of SA formed dense and well-ordered leaf-like crystals. With the dilution of TWA solution, sparse needle-like crystals were formed, while with the addition of the same amount of FWI solution, amorphous film was formed. (**B**) Bottom layers were different saturations of SA, from left to right: 90%, 50%, 10%, diluted by TWA (top-row) and FWI (bottom-row) solution separately. Middle layer was the mixture of analyte and internal standard protein, top layer was the saturated SA. (**C**) Bottom layer was the saturated SA, middle layer was the mixture of analyte and internal standard protein, top layer was the 10 % saturation SA. Scale bar: 500 μm (zoom in) and 200 μm (zoom out). The black ring shown the area of the sample spot on the MALDI-plate.
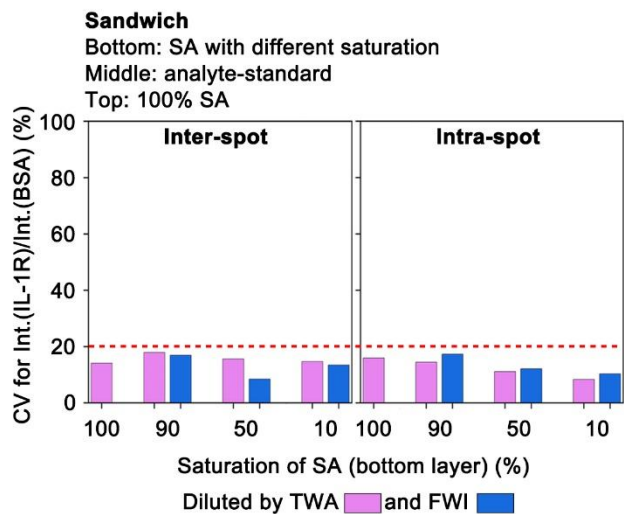
**Figure S5.** Coefficient of variance (CV) of the peak integral ratio of analyte (IL-1R) to internal standard (BSA) calculated under sandwich deposition method. Four different saturations (100%, 90%, 50%, and 10%) of SA (on the bottom layer or top layer) diluted by TWA (pink) and FWI (blue), separately, were tested. Inter-spot data was collected from nine spots from each of the deposition way. Intra-spot data was collected from nine different parts of one spot. CV values less than 20% were considered as stable data (below red dash line).
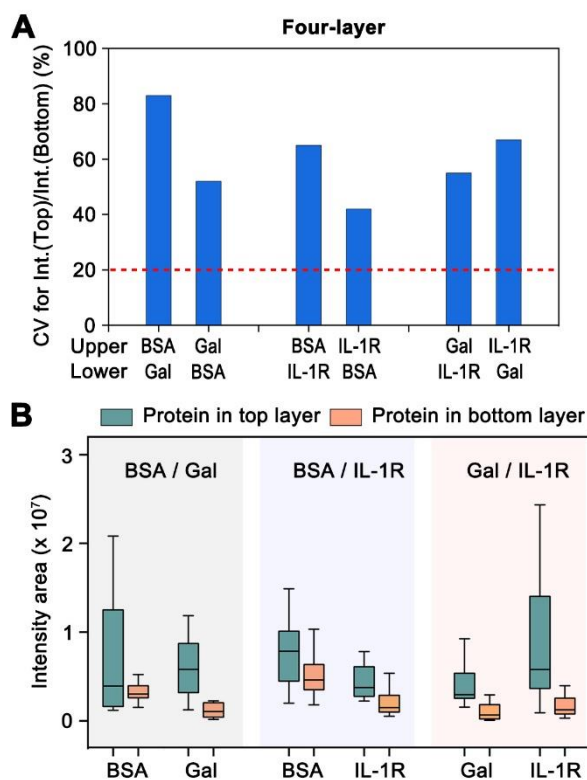


**Figure S6. (A)** CV of the peak intensity ratio (top-layer protein against bottom-layer protein) using four-layer deposition method. Bottom layer was 50% SA (diluted by FWI), top layer was 100% SA. Equimolar IL-1R, BSA and Gal were paired with each other, and each protein was placed on the second and third layer respectively. Each CV value was calculated from nine independent repeat experiments of each deposition method. **(B)**

91 Boxplots showing peak intensities (25th-75th percentile with the median) of each protein when placed on the
92 top (green) and at the bottom layer (orange) respectively. The error bar corresponds to $1.5 \times IQR$. $n = 9$
93 independent samples. CV values less than 20% were considered as stable data (below red dash line).
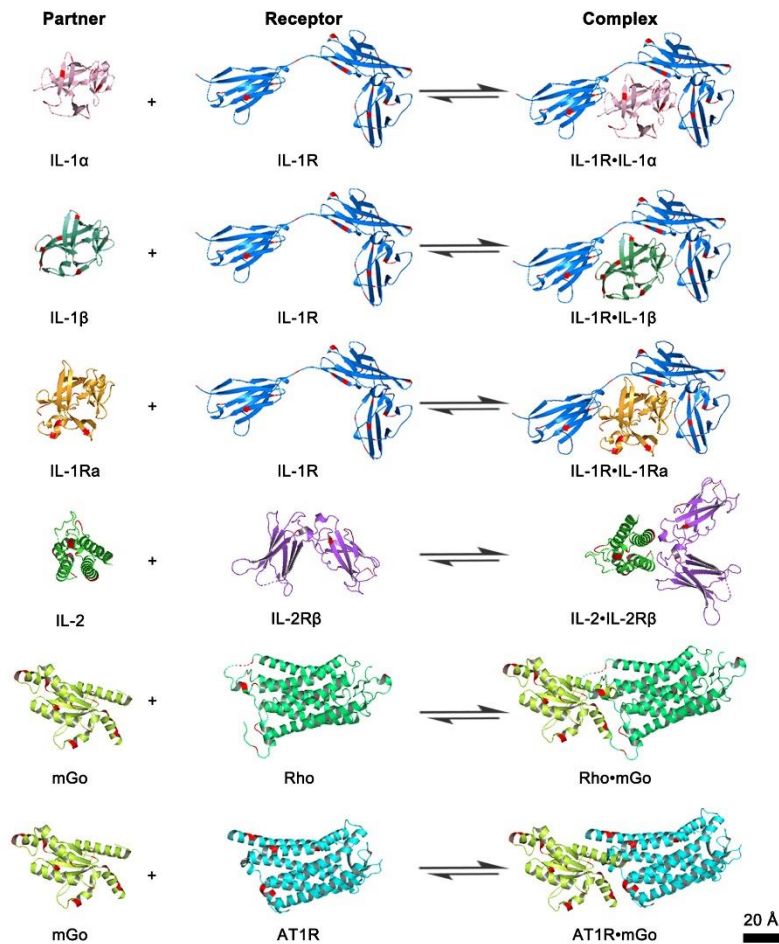


94

95 **Figure S7.** Three-dimensional structural models of the tested receptors and partners, and their formed complexes.
96 The position of the lysine residues in the proteins shown that all the protein complexes are in the crosslinking
97 range of BS(PEG)$_9$. IL-1α (PDB: 5UC6), IL-1β (PDB: 4DEP), IL-1Ra (PDB: 1IRA), IL-1R (PDB: 1IRA), IL-2
98 (PDB: 5B5I), IL-2Rβ (PDB: 5B5I), Rho (PDB: 2I37), AT1R (PDB: 6DO1), and mGo (PDB: 6G79). Scale bar:
99 20 Å.

100
101
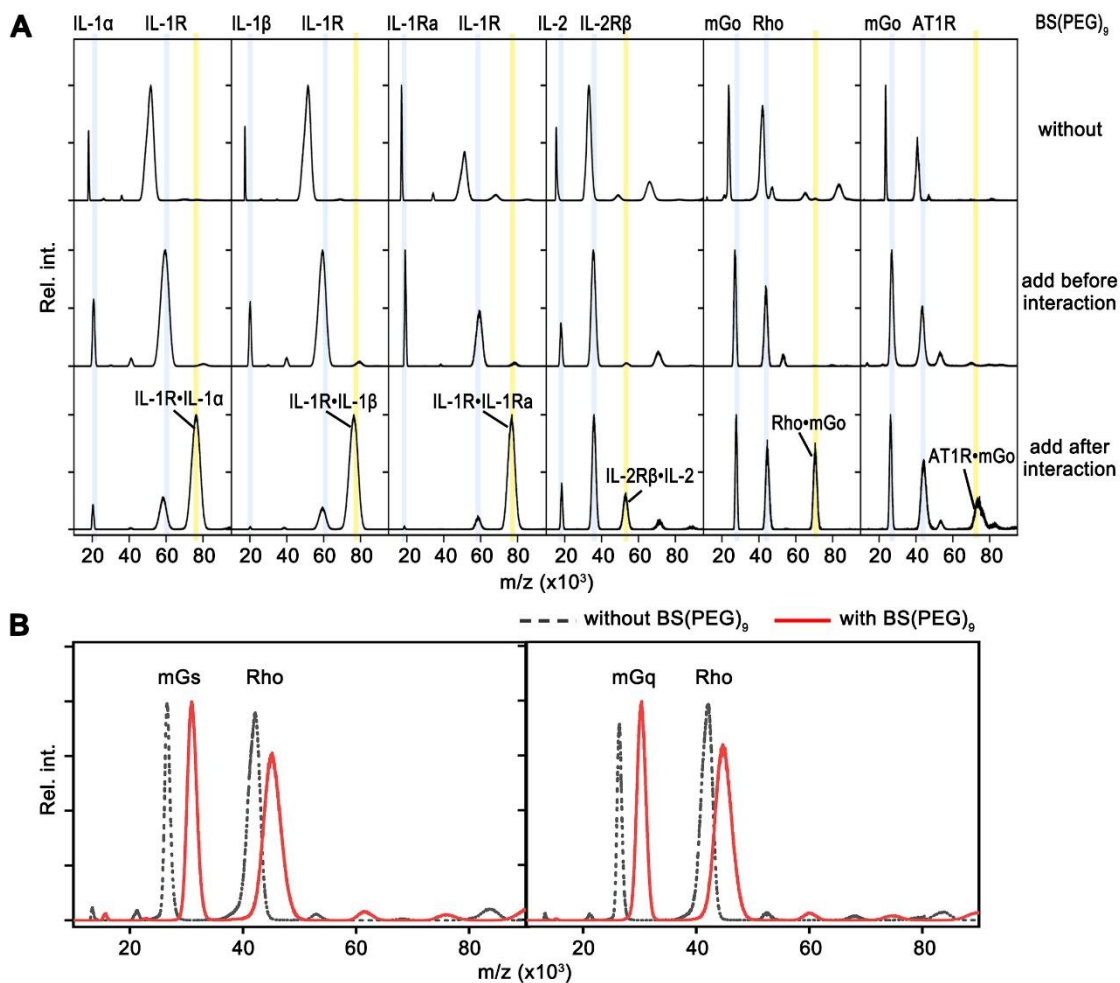
**Figure S8. (A)** Mass spectra of the formation of receptor•partner complexes (from left to right: IL-1R•IL-1α, IL-1R•IL-1β, IL-1R•IL-1Ra, IL-2Rβ•IL-2, Rho•mGo, and AT1R•mGo) at the reaction equilibrium state, top spectrum: without the addition of BS(PEG)$_9$, middle spectrum: pre-treated the receptor and partner protein with BS(PEG)9 for 5 min, respectively, before mixed them together, bottom spectrum: added the BS(PEG)$_9$ after the reaction reached equilibrium. Grey lines: protein monomers, yellow lines: protein complexes. **(B)** Mass spectra of the interaction between mini-type Gs protein (mGs) and Rho, mini-type Gq protein (mGq) and Rho, without crosslinking (black dash line) and with crosslinking (red line). No protein complexes were formed.

## Derivation of the formula for calculating the K$_d$ value

Receptor-partner interactions as equilibrium phenomena as follows:

Receptor•Partner $\rightleftharpoons$ Receptor + Partner
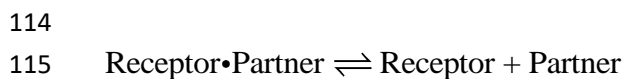
Abbreviated as:

R•P $\rightleftharpoons$ R+ P

Accordingly, the following equilibrium constant holds.

S8

119 $$K_d = \frac{[R][P]}{[R \bullet P]}$$

120 Here, $K_d$ is the so-called "dissociation constant"

121 When the concentration of the receptor ($[R]_0$) is present near Kd is close to $K_d$,

122 $$K_d = \frac{[R][P]}{[R \bullet P]} = \frac{([R]_0 - [R \bullet P])([P]_0 - [R \bullet P])}{[R \bullet P]}$$

123 $$K_d = \frac{[R]_0 \cdot [P]_0 - ([P]_0 + [R]_0)[R \bullet P] + [R \bullet P]^2}{[R \bullet P]}$$

124 $$K_d[R \bullet P] = [R]_0 \cdot [P]_0 - ([P]_0 + [R]_0)[R \bullet P] + [R \bullet P]^2$$

125 $$0 = [R]_0 \cdot [P]_0 - ([P]_0 + [R]_0 + K_d)[R \bullet P] + [R \bullet P]^2$$

126 The last equation is a second order polynomial in which one can solve for "x", [R•P], using the
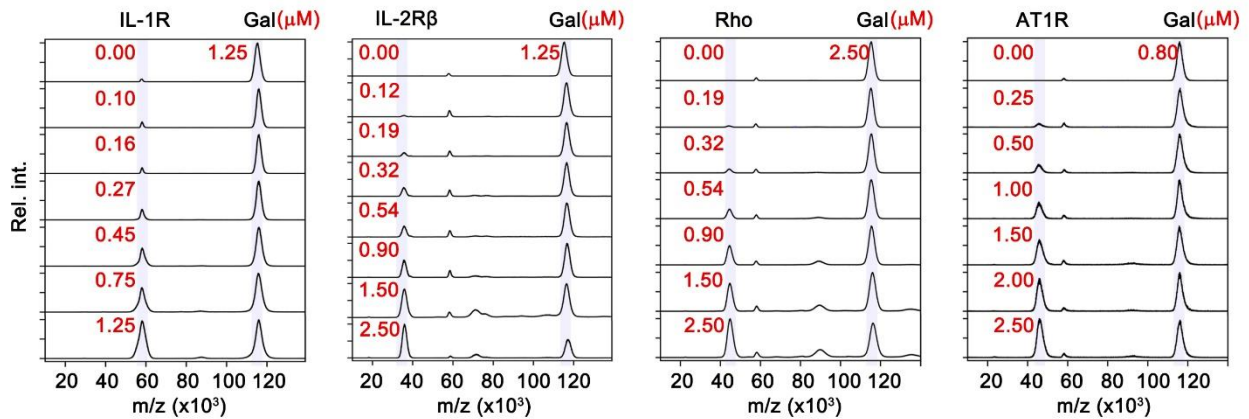127 quadratic equation.

128 $$[R \bullet P] = \frac{([P]_0 + [R]_0 + K_d) - \sqrt{([P]_0 + [R]_0 + K_d)^2 - 4 \cdot 1 \cdot [R]_0 \cdot [R]_0}}{2 \cdot 1}$$

129 Then we can get the following equation,

130 $$\frac{[R \bullet P]}{[R]_0} = \frac{([P]_0 + [R]_0 + K_d) - \sqrt{([P]_0 + [R]_0 + K_d)^2 - 4 \cdot [R]_0 \cdot [R]_0}}{2 \cdot [R]_0}$$

131 The applicable condition of this formula is when $K_d$ is less than ten times the total receptor
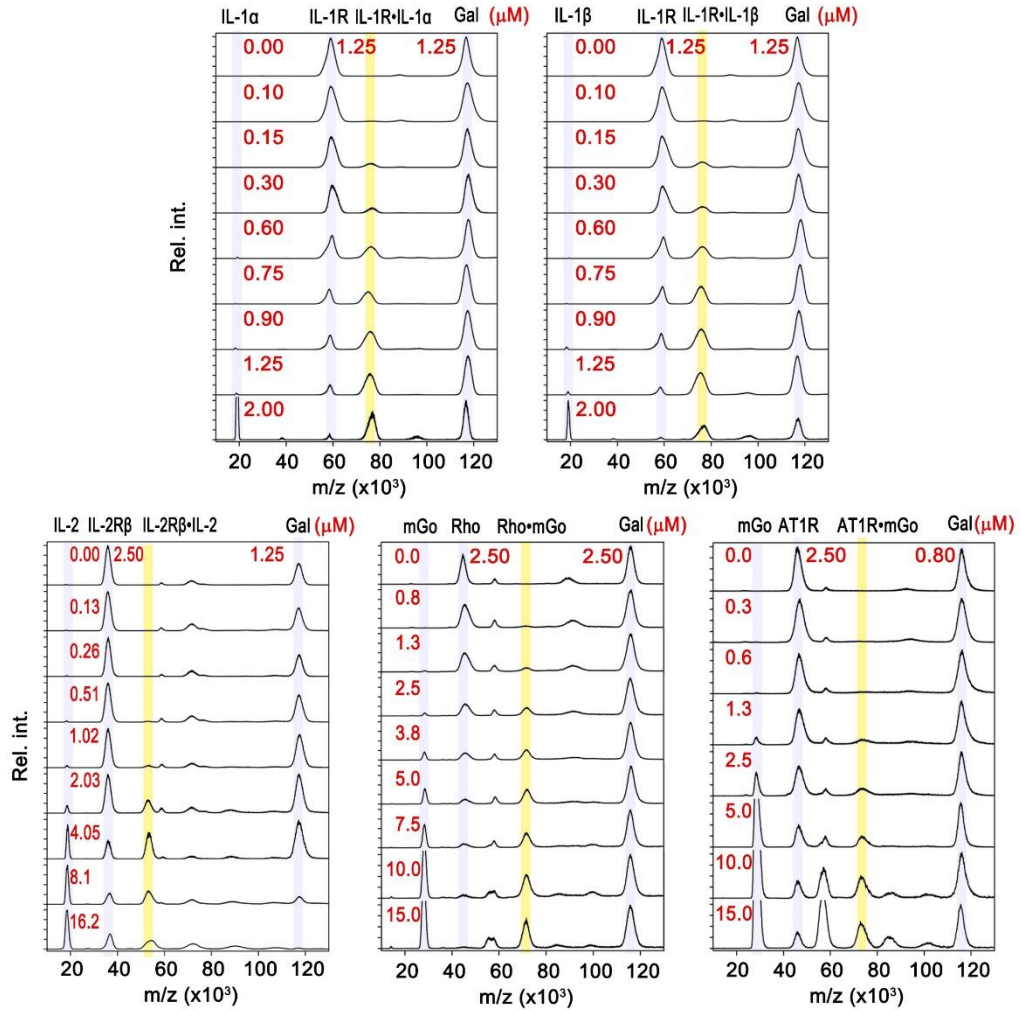132 concentration.

133

134



135 **Figure S9.** Gal normalized mass spectra of the receptors (from left to right: IL-1R, IL-2Rβ, Rho, AT1R) with
136 different concentrations.

137

**Figure S10.** Mass spectra of the formation of receptor•partner complexes (from left to right, top to bottom: IL-1R•IL-1α, IL-1R•IL-1β, IL-2Rβ•IL-2, Rho•mGo, and AT1R•mGo) with the titration of IL-1α, IL-1β, IL-2R, mGo, and mGo (from left to right, top to bottom). Gal was used as the internal standard protein. Grey lines: protein monomers, yellow lines: protein complexes.